# Enabling LAAS Airport Surface Movement: Mitigating the Anomalous Ionospheric Threat

Young Shin Park, Sam Pullen, and Per Enge
Dept. of Aeronautics and Astronautics
Stanford University
Stanford, USA
yspark@stanford.edu

***Abstract*—The Local Area Augmentation System (LAAS) can be used for both precision approach and Differentially Corrected Positioning Service (DCPS) applications. Through its support of DCPS, the LAAS Ground Facility (LGF) is required to meet the integrity requirements of all other operations that could use the LAAS VHF Data Broadcast (VDB). Our previous work [1,2,3] demonstrated that the existing DCPS integrity requirements cannot be met by CAT I LAAS without changes to both the definition of DCPS integrity [4,5] and the airborne receiver requirements [6]. One of the implications is that some future applications of LAAS that planned to use DCPS, such as airport surface movement, cannot be supported by DCPS with the CAT I LAAS architecture. However, if airport surface movement is defined as a separate operation, it could be supported by the existing LGF geometry screening that mitigates the anomalous ionospheric threat for CAT I precision approach. The only change needed would be to increase $\sigma_{pr\_air}$ in airborne equipment to bound the higher multipath errors in the airport surface environment. Confirming this hypothesis requires a more-intensive study of the requirements of airport surface movement and is the subject of this paper. If LGF geometry screening itself cannot support airport surface movement, the results in this paper include additional aircraft geometry screening proposed in [2] to lower the Maximum Acceptable Error (MAE) to a usable level while maintaining useful availability.**

***Keywords-GBAS; LAAS; DCPS; airport surface movement; anomalous ionosphere***

## I. INTRODUCTION

The Local Area Augmentation System (LAAS) is primarily focused on supporting precision approach but can also be used for a variety of other applications that are known as Differentially Corrected Positioning Service (DCPS) applications. A typical LAAS-equipped airport is illustrated in Fig. 1. There are four reference receivers around the LAAS Ground Facility (LGF), which does the central processing and determination of corrections that are transmitted via the VHF Data Broadcast (VDB) antenna. CAT I precision approach availability is typically evaluated at 6 kilometers away from the centroid of the LGF reference receivers, which represents the maximum separation of the CAT I Decision Height (DH) for most airports [7]. Ten nautical miles (18.5 kilometers) farther out along this approach direction marks the boundary of the Precision Approach Region (PAR).

DCPS is broadly composed of (but is not limited to) three operations. The first operation is terminal-area navigation for the aircraft in the region from the PAR to 45 kilometers away from the LGF. The second operation is enroute navigation for aircraft passing over the airport that can receive and make use of the LAAS VDB. The third operation is airport surface movement for aircraft on airport taxiways (and thus quite close to the LGF centroid). Note that the VDB is required to provide coverage out to 45 kilometers assuming a 3-degree glideslope for precision approaches. At higher altitudes, aircraft will receive the VDB at significantly further distances.

Through its support of DCPS, the LAAS Ground Facility is required to meet the integrity requirements of all other operations that could use the LAAS VDB. CAT I precision approach is approved under anomalous ionospheric conditions (the most constraining threat) for at least a 6-kilometer separation. The current LAAS requirements for DCPS integrity are that position errors should be bounded by the corresponding protection levels to the $10^{-7}$-per-hour probability level, regardless of the size of the error [4,5]. Our previous work [1] showed that the existing DCPS integrity requirements cannot be met by CAT I LAAS without changes to both the definition of DCPS integrity [4,5] and the airborne receiver requirements [6].

Our previous paper [2] identifies the changes that are required and recommends specific sets of alternatives. One of its conclusions is that some future applications of LAAS that planned to use DCPS, such as airport surface movement, cannot be supported by DCPS with the CAT-I LAAS architecture. It suggests one important further change to the LAAS avionics requirements. The current LAAS MOPS forbids use of the LAAS Position/Velocity/Timing (PVT) outputs if DCPS is not enabled by the LGF [6]. As this paper points out, it will not support all applications that can make use of the PVT outputs, even if DCPS is enabled. Therefore, the PVT outputs should be "de-linked" from DCPS so that they can be used independently. PVT applications that cannot be supported by DCPS should be defined as separate applications of LAAS in the same manner as precision approach.

SCPNT and the FAA LAAS Program Office

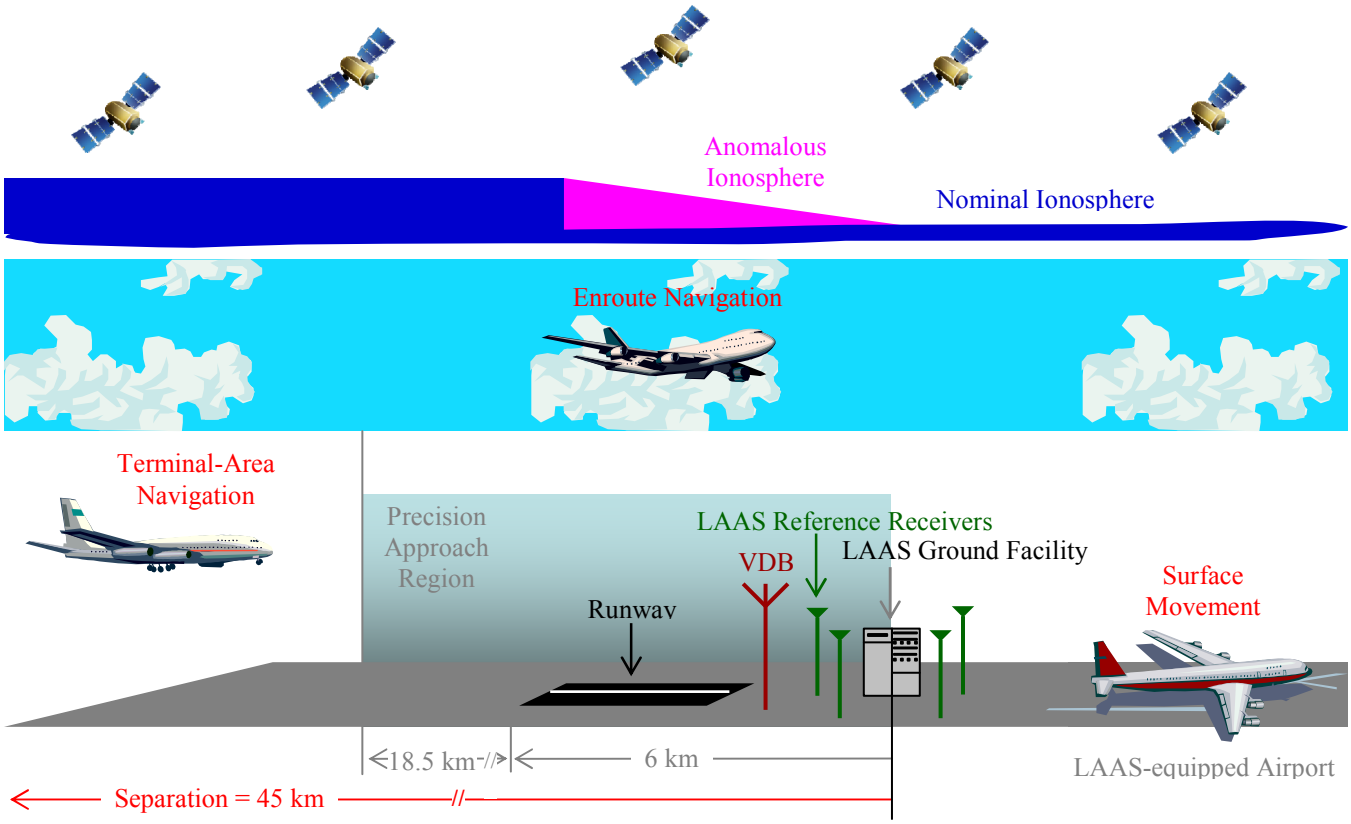


Figure 1. Operations included in DCPS at a LAAS-equipped airport.

Our original hypothesis was that, if airport surface movement is defined as a separate operation, it would be supported by the existing LGF geometry screening that mitigates the anomalous ionospheric threat for CAT I precision approach. The primary adjustment needed would be to increase the airborne $\sigma_{pr\_air}$ value if needed to bound the higher multipath errors expected in the airport surface environment (as opposed to an aircraft in flight). Confirming this hypothesis required a more-intensive study of the requirements on airport surface movement and is the subject of this paper. If LGF geometry screening itself cannot support airport surface movement, the results in this paper include additional aircraft geometry screening proposed in [2] to lower the Maximum Acceptable Error (MAE). Since it is not clear what level of MAE corresponds to a given airport-surface operation, our goal is to minimize the achievable MAE (and thus Horizontal Alert Limit, or HAL) while maintaining useful availability.

## II. Simulation Procedure

### A. *Simulation of HPE and HPL for Airport Surface Movement*

The simulation procedure used to obtain Horizontal Position Errors (HPEs) and the corresponding Horizontal Protection Levels (HPLs) for DCPS has been expanded from the methodology in [1,2,3] and is shown in Fig. 2. One day of geometries with five-minute time updates and a 5-degree visibility mask angle at Memphis International Airport (MEM) is used to generate all-in-view, all 1-satellite-out ($N$–1), all 2-satellite-out ($N$–2), etc., down to all 4-satellite subset geometries. The variable $N$ represents the number of visible satellites in the geometry (which are all assumed to be approved for use by the LGF). The maximum supported distance from LGF to user, defined as $D_{max}$ and included in the information broadcast by the VDB [6,8], is set by the service provider. A typical value for $D_{max}$ is 45 kilometers (the maximum coverage of the VDB at approach altitude), and LGF-to-user separations of 0 to 6 kilometers are used for the simulation of airport surface movement.

Worst-case GPS range errors from the anomalous ionospheric threat model for the Conterminous U.S. (CONUS) [9] are applied to all individual satellites in all allowed subset geometries, one satellite at a time. Anomalous ionospheric range errors applied to individual satellites are proportional to the distance from LGF to user with the addition of a bias due to an assumed aircraft velocity in the direction of the ground facility. In this paper, for airport surface movement, a speed of 10 m/s (about 19.4 knots, or 22.4 mph) is used because it is a typical aircraft velocity at a distance of 6 km from an airport, although the actual speed could be different according to the particular airport surface movement operation being conducted.

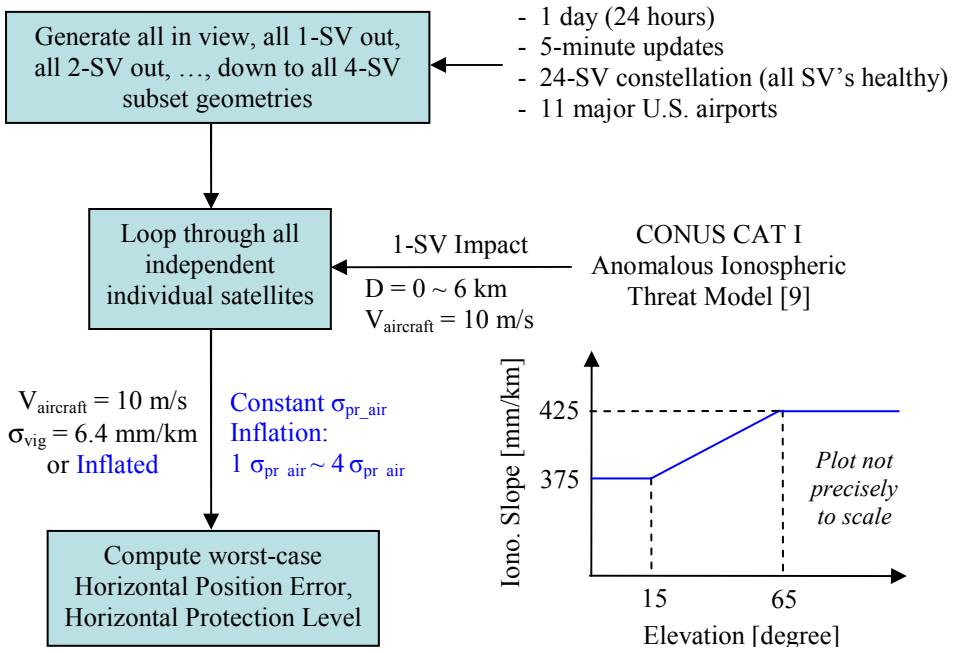


Figure 2. Airport surface movement simulation procedure to generate worst-case errors under ionospheric anomalies.

The nominal ionospheric gradient parameter, the standard deviation of the vertical ionosphere gradient or $\sigma_{vig}$, may vary due to the LGF geometry screening needed to protect CAT I precision approach, which is briefly described in the next section. Here, the nominal (uninflated) $\sigma_{vig}$ of 6.4 millimeters per kilometer is used to compute both HPE and the uninflated HPL, and a specific value of inflated $\sigma_{vig}$ for each epoch obtained by the real-time sigma-inflation algorithm used for precision approach is used to compute the inflated HPL.

The standard deviation of the aircraft contribution to the total pseudorange error, $\sigma_{pr\_air}$, includes airborne receiver noise and a standard allowance for airframe multipath. The performance of the airborne subsystem is defined in terms of Airborne Accuracy Designators (AAD). Currently two AAD (A and B) are defined in and empirical expressions can be obtained from [5,6]. In these simulations, the more conservative model (AAD A) is used for computing errors and uninflated HPL, while AAD B is used for computing inflated HPL at an aircraft. For both of them, Airframe Multipath Designator (AMD) A is used for the airborne $\sigma_{multipath}$ defined in [5,6]. A broadcast multiplier (unitless) for computation of the ephemeris error position bound for the LAAS positioning service, $K_{md\_e\_POS\_hrz}$, of 5.085, and an ephemeris decorrelation parameter, or "P-value" ($P_k$), of 0.00018 meters per meter, are used [6,8]. HPE, HPL, and inflated HPL are computed as described in [6,8], and the largest HPE and corresponding HPL and inflated HPL are stored for each subset geometry generated by the satellite geometry simulation described above.

### *B. Real-Time $\sigma_{vig}$-Inflation Simulation for precision approach*

The simulation used to establish real-time inflation factors for $\sigma_{vig}$ to protect CAT-I precision approach is based on the methodology in [7] and is modified to fit the current CAT I LAAS operational design. Subset geometries are generated for CAT I in the same manner as for DCPS except that valid airborne geometries are limited to no more than two satellites fewer than the *N* satellites approved by the LGF (*N*–2). In addition, geometries whose inflated Vertical Protection Levels (VPLs) are above the CAT I Vertical Alert Limit (VAL) of 10 meters are "screened out" (i.e., made unavailable for use in the simulation). The assumed distance from LGF to user at the 200-ft CAT I decision height is set to be 6 kilometers [7].

Unlike airport surface movement (or DCPS) in this paper, the worst-case ionosphere impact for precision approach must be evaluated over all independent pairs of satellites in each subset geometry. Ionosphere-induced range errors for CAT I are determined by closed-form equations based upon the parameters from the ionospheric anomaly threat model for CONUS. These expressions, whose key parameter is the ionosphere front velocity, are modified from [10]. The LGF uses a Code-Carrier Divergence (CCD) Monitor to detect anomalous ionospheric activity [11]. However, for this monitor to detect hazardous spatial gradients, the relative velocity ($\Delta v$ (km/s)) between two LGF Ionosphere Pierce Point (IPP) velocities and projected onto the direction of the ionosphere front velocity must be significantly non-zero. For smaller relative velocities, the CCD monitor does not alert, and the resulting undetected user errors can be large (albeit very rare).

The closed-form range error models used in this simulation can be summarized as follows [3].

*1) Slow Ionosphere Front Speed:* There is no CCD detection in these cases. The error (ε (m)) induced by the ionosphere is proportional to the separation between the GBAS ground facility and the approaching aircraft. This relationship is expressed as:

$$\Delta v < \frac{0.0229\,[\text{m/s}]}{\min\left[\frac{50\,[\text{m}]}{W}, G\right]}, \quad \Delta v < 0.11\,[\text{km/s}] \tag{1}$$

$$\varepsilon = \min\left[\frac{50[\text{m}]}{W}, G\right] \times \left(x + 2\tau v_{aircraft}\right) \tag{2}$$

where,

$W$: Width of the ionosphere front (km);
G: Gradient or "slope" of the ionosphere front through which the IPP passes through (m/km);
τ: 100-second smoothing time of the Carrier-Smoothing filter used by LAAS (s);
$v_{aircraft}$: Velocity of the user aircraft during its final approach segment (assumed to be a constant 0.070 km/s in this paper) (km/s);
$x$: Distance between the LGF and the user (conservatively assumed to be 6 km in this paper) (km).

*2) Moderate Ionosphere Front Speed:* In these cases, the CCD monitor alerts for some conditions within this range of relative speeds. Consequently, the errors that users could suffer begin to decrease. Under the CONUS threat model, the maximum differential range error the user would suffer is no greater than 4 meters.

$$\Delta v < \frac{0.0229\,[\text{m/s}]}{\min\left[\frac{50\,[\text{m}]}{W}, G\right]}, \quad \Delta v < 0.11\,[\text{km/s}] \tag{3}$$

*3) Fast Front Ionosphere Speed:* In these cases, The CCD monitor alerts with a very small missed-detection probability. Under the CONUS threat model, the maximum range error that users could potentially suffer is no greater than 2.5 meters.

$$\Delta v > 0.11\,[\text{km/s}] \tag{4}$$

The broadcast multiplier (unitless) for computation of the ephemeris error position bound for Category I precision approach, $K_{md\_e\_CAT1}$, of 5.085, and the same $P_k$ of 0.00018 m/m, are used to get Ionosphere-induced-Error-in-Vertical (IEV), VPL, and required inflation factors for $\sigma_{vig}$ [7] as needed. Note that the multiplier (unitless) which determines the probability of missed detection, $K_{md}$, of zero is used in IEV because IEV only includes the impact of ionospheric anomalies. The applied ionospheric range errors are all positive as expressed before and are actually magnitude of actual errors. To take care of it, four possible combinations of range errors of satellites $k_1$ and $k_2$ are considered as below.

$$IEV_{k1,k2,1} = |S_{verrtical,k1}\ \varepsilon_{k1,positive} + S_{vertical,k2}\ \varepsilon_{k2,positive}| \tag{5}$$

$$IEV_{k1,k2,2} = |S_{vertical,k1}\ \varepsilon_{k1,positive} + S_{vertical,k2}\ \varepsilon_{k2,negative}| \tag{6}$$

$$IEV_{k1,k2,3} = |S_{vertical,k1}\ \varepsilon_{k1,negative} + S_{vertical,k2}\ \varepsilon_{k2,positive}| \tag{7}$$

$$IEV_{k1,k2,4} = |S_{vertical,k1}\ \varepsilon_{k1,negative} + S_{vertical,k2}\ \varepsilon_{k2,negative}| \tag{8}$$

where $S_{vertical}$ is the row of the weighted-least-squares projection matrix corresponding to the vertical position component [6]. The largest of these four vertical errors is the worst-case IEV. Fig. 3 shows the Maximum-Ionosphere-induced-Error-in-Vertical (MIEV) per epoch.

In order to ensure that VAL bounds the MIEV for all usable "subset" geometries, real-time-sigma-inflation beyond the nominal sigma value of 6.4 mm/km is performed when needed using the pre-computed and stored values of IEV and VPL for CAT-I precision approach. This simulation procedure is based on Fig. 10 and Fig. 11 in [7]. A single epoch is considered as an example to briefly explain the concept of $\sigma_{vig}$ inflation. If IEV for a particular subset geometry is above the tolerable error limit (28.78 m) derived from the Obstacle Clearance Surface (OCS) at the CAT-I decision height [12], $\sigma_{vig}$ is increased until the VPL for that geometry (based upon the inflated $\sigma_{vig}$) is above VAL; thus that problematic geometry will be screened out (made unavailable) by the VPL check at the aircraft. This sigma-inflation procedure is repeated until all subset geometries with IEV exceeding 28.78 m are made unusable, meaning that the "maximum IEV" (MIEV) of the remaining "usable" geometries is no greater than 28.78 m. The resulting value of $\sigma_{vig}$ per each epoch, as shown in Fig. 4, is fed into the airport surface movement (or DCPS) simulation to compute inflated HPL for users not limited to the CAT-I approach phase of flight.

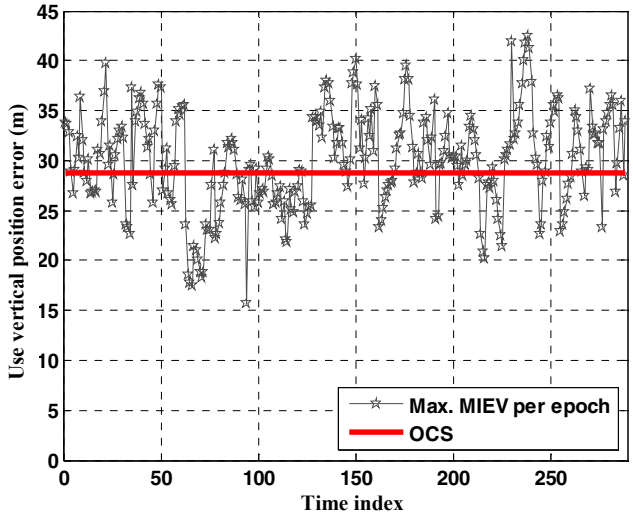


Figure 3. MIEV simulation results of all the subset gemetries for precision approach at Memphis using RTCA 24-SV constellation.

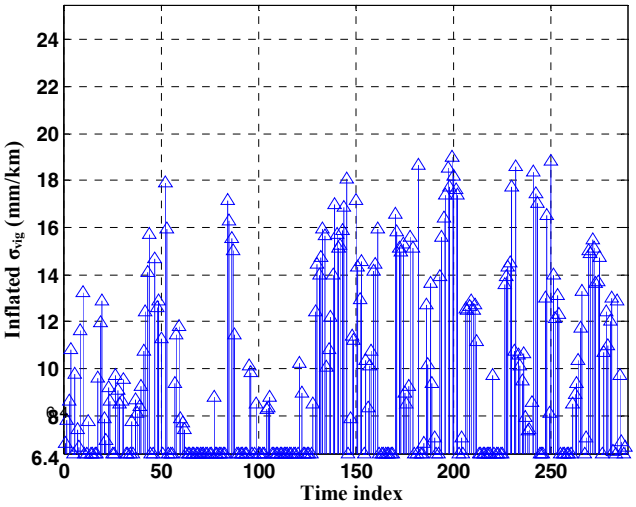


Figure 4. Real-time inflated $\sigma_{vig}$ for precision approach at Memphis.

## III. DCPS INTEGRITY

Previous results for DCPS integrity in the operational context [3] are shown here to highlight the difficulty of supporting airport surface movement within DCPS. The scenario shown here represents terminal-area navigation: the aircraft velocity is 130 meters per second at 45 kilometers apart from the LGF. Simulated HPEs which this aircraft would suffer from anomalous ionospheric residual errors, and the corresponding HPLs which it would calculate using real-time LGF $\sigma_{vig}$ inflation, are shown in Fig. 5. The cyan oval indicates the zone of nominal errors for all-in-view geometries. The black dots represent anomalous ionospheric errors for all-in-view geometries, and other dots denote these errors for all subset geometries down to 4 satellites.

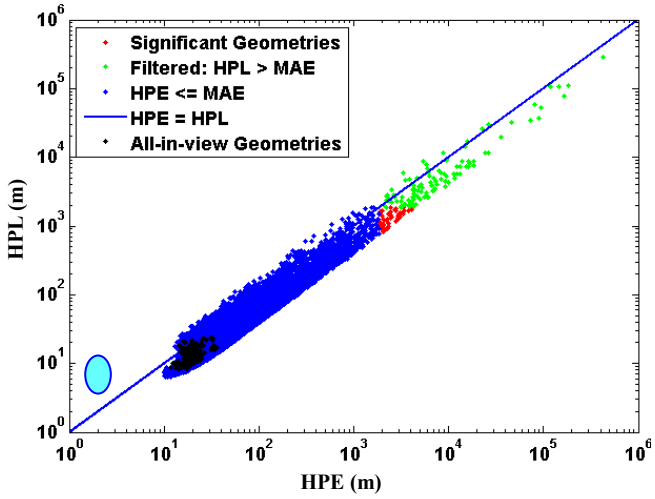


Figure 5. Example result of DCPS (terminal area navigation) at Memphis: inflated $\sigma_{vig}$.

Note that HPE is acceptably large up to the order of $10^5$ meters only because no advanced HAL-HPL check to screen out bad geometries is performed, since HAL is not specified in DCPS yet. Along the blue line, HPE is the same as HPL. In the upper triangle above this blue line, HPE is bounded by HPL, while HPE is not bounded by HPL in the lower triangle below it. The blue dots represent geometries with acceptable errors when the allowed MAE is 1852 meters (1 nautical mile). The green dots refer to geometries filtered by their HPLs, since the aircraft would screen out all the geometries whose HPL is greater than the MAE. The red dots denote significant geometries that might pose an anomalous ionospheric threat to DCPS, and DCPS integrity cannot be met under anomalous ionosphere unless these points are made unavailable by some other means.

## IV. LGF SIGMA INFLATION

If DCPS cannot be enabled, then any operations that provide the positioning service including airport surface movement can't be enabled. However, since airport surface movement is operated near LGF and an aircraft moves with slow speed, anomalous ionospheric errors are smaller than the errors in other operations of DCPS. If airport surface movement is defined as a separate operation from DCPS, it might be supported by the existing LGF geometry screening implemented to protect the CAT I precision-approach operation.

Since an aircraft in airport surface movement is on the ground, it suffers from higher multipath errors than while in flight, as additional signal reflections come from the ground, other aircraft or vehicles, and nearby buildings. In addition to real-time LGF $\sigma_{vig}$ inflation, a larger value of $\sigma_{pr\_air}$ inflation is likely needed to bound these higher multipath errors during airport surface environment. In this paper, the application of higher values of $\sigma_{pr\_air}$ takes the form of "inflation" of the existing $\sigma_{pr\_air}$ model by a constant multiplier. Since the degree of $\sigma_{pr\_air}$ inflation required is not yet known, several multiplier values are investigated.

### A. *Impact of LGF Sigma Inflation*

For simulation of LAAS-guided surface movement in this paper, all subset geometries down to 4 satellites are considered, and HPE expresses the worst-case ionospheric error only. As with the precision approach IEV, no nominal error contribution (including the projected nominal impact of multipath in the airport surface environment) is added to it.

Fig. 6 shows the impact of LGF $\sigma_{vig}$ inflation on HPL for LGF-to-user separation of 6 kilometers. While HPL in Fig. 6(a) is computed using a fixed, uninflated $\sigma_{vig}$ value of 6.4 millimeters per kilometer, HPL in Fig. 6(b) is computed using the inflated $\sigma_{vig}$ values shown in Fig. 4. Some geometries unprotected by HPL in Fig. 6(a) and thus represented by red dots become protected geometries (HPL ≥ HPE) denoted by green dots in Fig. 6(b).

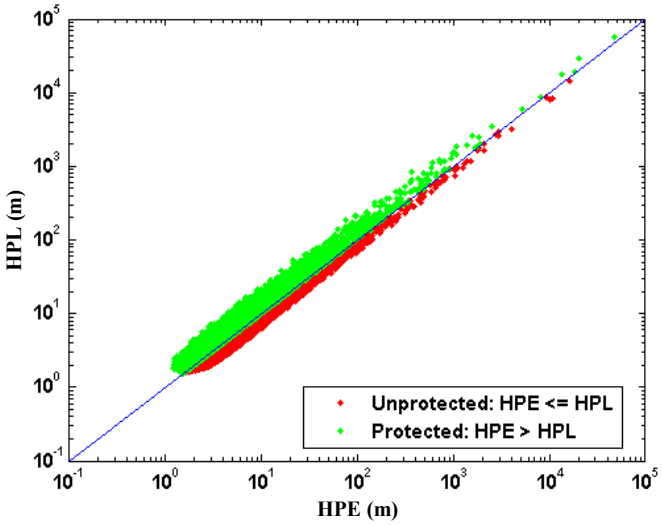


(a)

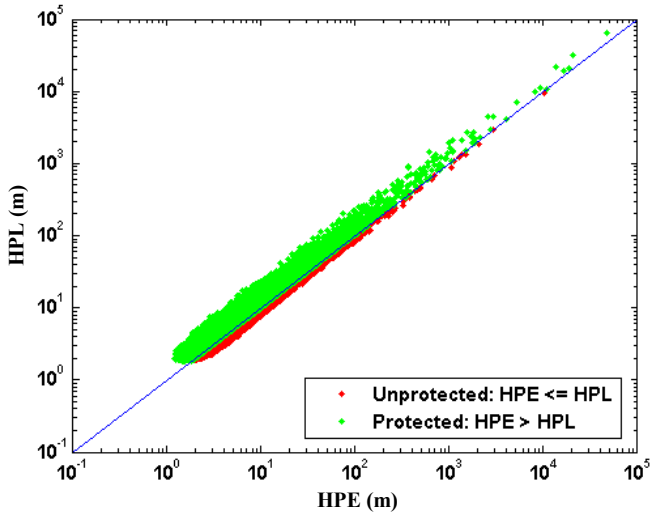


(b)

Figure 6. Impact of LGF $\sigma_{vig}$ inflation on HPL: (a) no inflation of $\sigma_{vig}$ and $\sigma_{pr\_air}$, (b) inflation of $\sigma_{vig}$ and no inflation of $\sigma_{pr\_air}$.

The sensitivity of HPL to constant airborne $\sigma_{pr\_air}$ inflation (to bound larger multipath errors) is demonstrated from Fig. 6(b) to Fig. 7. HPL in Fig. 7 is computed using a constant $\sigma_{pr\_air}$ value inflated by factor of 2 in addition to the LGF-inflated $\sigma_{vig}$ values. All geometries left unprotected in Fig. 6(b) and thus represented by red dots are moved to the green-dot protected region in Fig. 7.

To clarify which surface-movement scenarios are protected by HPL bounding, maximum values of the HPE-to-HPL ratio for different combinations of $\sigma_{vig}$ and $\sigma_{pr\_air}$ for LGF-to-user separations of 0 to 6 kilometers are shown in Fig. 8. The blue triangles represent the scenario of no inflation in either $\sigma_{vig}$ or $\sigma_{pr\_air}$. The green circles represent the scenario of inflated $\sigma_{vig}$ and no inflation of $\sigma_{pr\_air}$, the red triangles represent no inflation of $\sigma_{vig}$ and $\sigma_{pr\_air}$ inflated by a factor of 2, and the cyan circles represent inflated $\sigma_{vig}$ and $\sigma_{pr\_air}$ inflated by a factor of 2. Note that the HPE values for the scenario of inflated $\sigma_{vig}$ and $\sigma_{pr\_air}$ inflated by a factor of 2, as shown by the cyan line are bounded by their corresponding HPLs. In other words, the HPE-to-HPL ratio always exceeds 1.0. This indicates that the airport surface movement integrity requirements can be met (for any definition of MAE or HAL) by CAT I LAAS using the current approach to LGF geometry screening and a doubling of $\sigma_{pr\_air}$. From now on, real-time LGF $\sigma_{vig}$ inflation is used in every simulation unless specified since it is required in today's LAAS and, as expected it makes the surface-movement integrity requirement easier to meet.

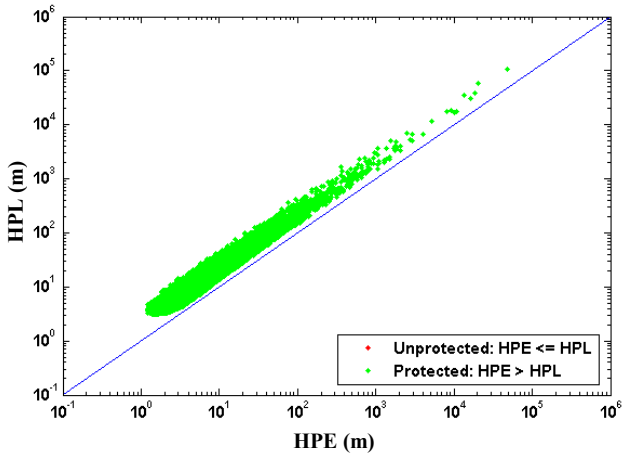


Figure 7. Impact of airborne $\sigma_{pr\_air}$ inflation on HPL: inflated $\sigma_{vig}$ and 2 $\sigma_{pr\_air}$.

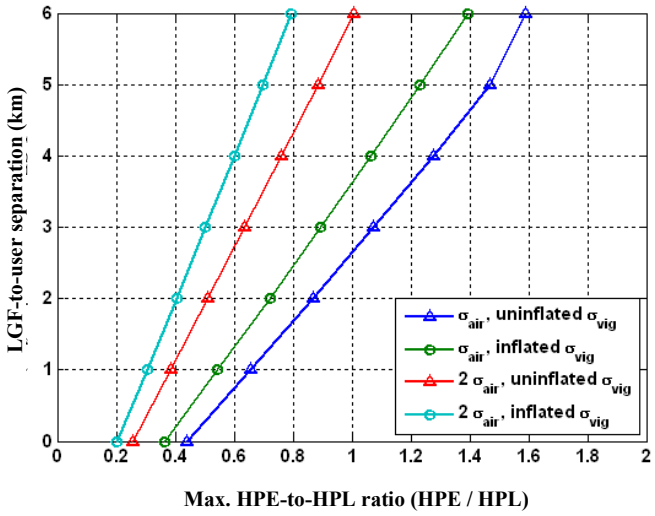


Figure 8. Scenarios protected by HPL bounding.

### B. *Availability Computation*

Availability is calculated from two different types of geometry sets in this paper. One is a set of all-in-view geometries only, and the other is a set of all-in-view geometries plus subset geometries with one satellite missing – these will be called "drill-down to one satellite out" geometries or "*N*–1 geometries" from now on. The latter geometry type is considered for the cases that one satellite is unhealthy or the signal from one satellite is lost because of other aircraft or vehicles, and nearby buildings Availability is obtained by counting how many geometries have HPLs less than or equal to MAE among the two geometry sets described above.

### C. *Availability Results*

The comparison of availability for these two types of geometries is shown in Fig. 9 for the LGF-to-user separation of 6 kilometers and the sigma-inflation scenario represented by the cyan line in Fig. 8. MAE for surface movement represents the same concept as VAL or HAL for precision approach and is evaluated for 3, 4, 5, 7.5, 10 meters, and higher with a 5-meter interval. The availability for all-in-view geometries only is 100% for an MAE of 7.5 meters or more and 94.44% for an MAE of 5 meters. On the other hand, the availability for "drill-down to one satellite out" or *N*–1 geometries is 97.76% for an MAE of 7.5 meters, 99.59% for 10 meters, and 100% for 25 meters or more. As expected, the availability for *N*–1 geometries is equal to or less than availability for all-in-view geometries. Therefore, availability evaluations in this paper report availability for *N*–1 geometries unless mentioned specifically. Availability values for additional parameter combinations are available in TABLE III of the Appendix.

Fig. 10 shows the sensitivity of MAE and availability to constant airborne $\sigma_{pr\_air}$ inflation for a LGF-to-user separation of 6 kilometers. The $\sigma_{pr\_air}$ value for a particular satellite elevation angle is inflated by factor of 1.5, 2, 3, and 4, and these cases are represented by blue, cyan, yellow, and red bars, respectively. For a multiplier of 1.5, MAE can be reduced to 5 meters with 91.82% availability and 7.5 meters with 99.55% availability. It can be reduced to 7.5 meters with 97.76% availability for a multiplier of 2, 10 meters with 96.58% for a multiplier of 3, and 15 meters with 98.58% for a multiplier of 4. Again, additional results are in TABLE III of the Appendix.

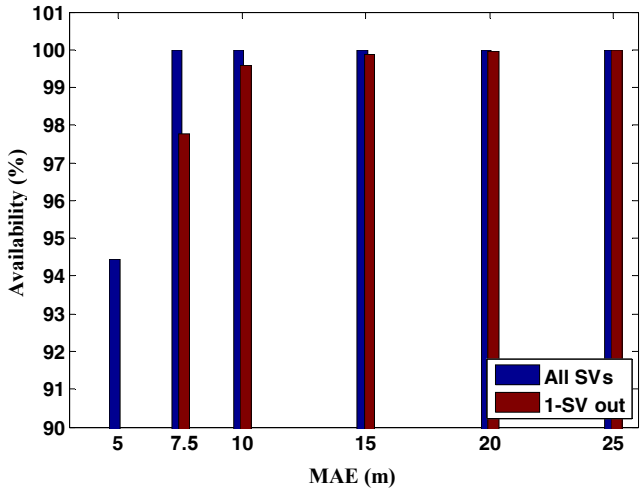


Figure 9. Availability for the scenario of inflated $\sigma_{vig}$ and 2 $\sigma_{pr\_air}$.

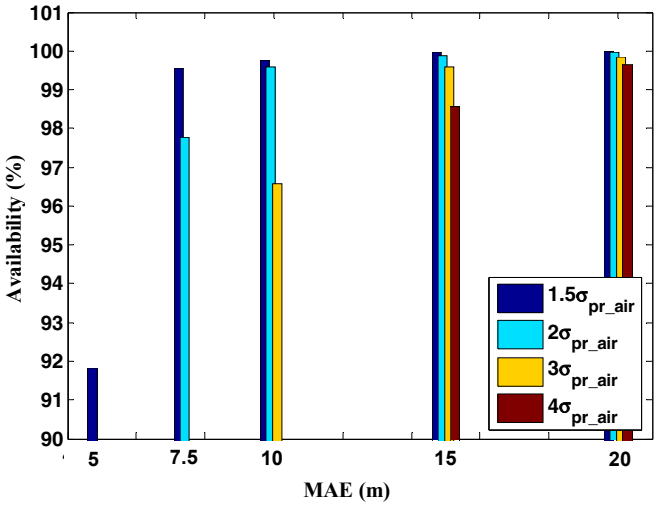


Figure 10. Sensitivity of MAE to airborne $\sigma_{pr\_air}$ inflation and its availability: inflated $\sigma_{vig}$.

## V. ADDITIONAL AIRBORNE GEOMETRY SCREENING

Fig. 8 is revisited to consider the scenarios where the maximum value of HPE-to-HPL ratio exceeds 1.0. One example of these scenarios is the case where the airborne $\sigma_{pr\_air}$ value does not need to be increased when the aircraft is on the ground. The other example is where the combination of a higher $\sigma_{pr\_air}$ value to bound larger multipath errors and a version of HPE that includes nominal errors (in addition to the worst-case ionospheric error) result in the HPE-to-HPL ratio sitting in the region where the maximum ratio is over 1.0. For those scenarios, the additional airborne geometry screening introduced in our previous work [2] is applied to protect integrity while lowering MAE to a usable level and maintaining a useful level of availability. Two types of airborne geometry screening rules have been evaluated. The first rule is limiting a "screening HAL" to less than the normal HAL or MAE that is dictated by safety concerns. The second rule is limiting the maximum absolute value of the range-to-horizontal position scalar, $|S_{horizontal}|$, where the matrix S is derived from the weighted pseudoinverse of the user's GPS geometry matrix [6]. In this section, the relatively difficult and unlikely combination of LGF $\sigma_{vig}$ inflation and no inflation of $\sigma_{pr\_air}$ is selected to demonstrate the capabilities of additional airborne geometry screening.

### A. Determination of Limits

In order to show how airborne geometry screening limits are determined, an example plot for the LGF-to-user separation of 6 kilometers is shown in Fig. 11(a). If MAE is set to be 10 meters, the significant geometries are shown by red dots in Fig. 11(a), can be seen more closely in Fig. 11(b). The required "screening HAL" is determined by the minimum HPL value among these significant geometries, and the maximum $|S_{horizontal}|$ is determined by the minimum value of $|S_{horizontal}|$ among them. Note that, where additional airborne screening is needed, either the screening HAL or the maximum $|S_{horizontal}|$ determined in this manner is sufficient – there is no need to implement both limits at the same time.

### B. Availability Computation

Availability is determined by counting how many geometries satisfy (9) for the screening HAL limit or (10) for the maximum $|S_{horizontal}|$ limit.

$$\{\text{HPL} \le \text{MAE}\} \cap \{\text{HPL} < \text{Screening HAL}\} \quad (9)$$

$$\{\text{HPL} \le \text{MAE}\} \cap \{|S_{horizontal}| < \text{Max. } |S_{horizontal}|\} \quad (10)$$

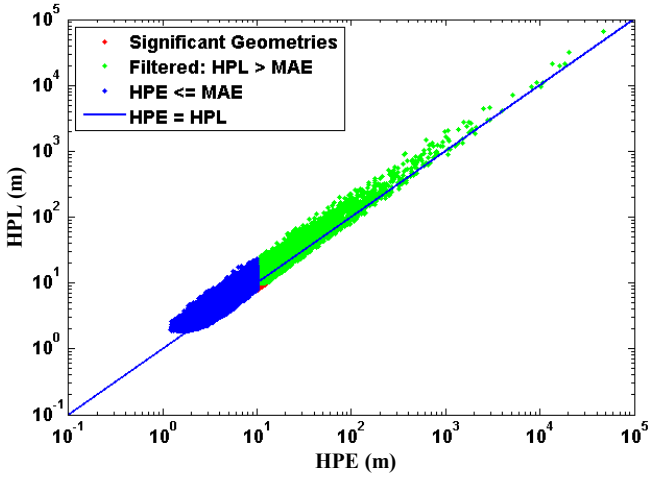


(a)

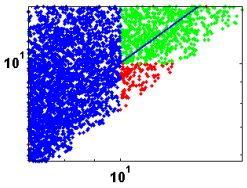

(b)

Figure 11. Example result of airport surface movement for 6-km separation: inflated $\sigma_{vig}$ and no inflation of $\sigma_{pr\_air}$.

### C. Availability Results

Fig. 12 shows availability as a function of MAE when a screening HAL is used for three LGF-to-user separations of 4, 5, and 6 kilometers. For a separation of 4 kilometers, 96.17% availability is achieved for an MAE of 4 meters by using a screening HAL of 3.99 meters. In other words, the aircraft should screen out all geometries whose HPL is more than the screening HAL of 3.99 meters to support the actual ("safety") HAL of 4 meters with the required integrity. In this case, the screening HAL is only slightly less than the actual HAL; thus the additional geometry restriction is very minor. In the same manner, MAE is reduced to 5 meters with 96.01% availability using a screening HAL of 4.11 meters for a 5-kilometer separation and is reduced to 7.5 meters with 99.47% availability using a screening HAL of 5.69 meters for a 6-kilometer separation. Screening limits and availabilities for additional scenarios are provided in TABLE I of the Appendix.

Availability with MAE when maximum $|S_{horizontal}|$ is used to screen airborne geometries for the same three separations is shown in Fig. 13. MAE can be reduced to 4 meters with 96.30% availability with a maximum $|S_{horizontal}|$ of 1.60 to protect integrity for the 4-kilometer separation. An availability of 94.59% is achieved for an MAE of 4 meters and a 5-kilometer separation by a maximum $|S_{horizontal}|$ of 1.35. Availability is 98.37% for an MAE of 5 meters and a separation of 6 kilometers using a maximum $|S_{horizontal}|$ of 1.47. Values for additional combinations are available in TABLE II of the Appendix. Comparing Fig. 13 to Fig. 12

suggests that limiting maximum $|S_{horizontal}|$ provides slightly better availability than the screening-HAL alternative.

The result shown in Fig. 14 gives availability for all-in-view geometries only. In Fig. 14, MAE is reduced to 3 meters with 96.53% availability by a maximum $|S_{horizontal}|$ of 1.20 for a 4-kilometer separation, with 94.44% availability by a maximum $|S_{horizontal}|$ of 1.01 for a 5-kilometer separation, and with 92.71% availability by a maximum $|S_{horizontal}|$ of 0.89 for a 6-kilometer separation. As before, values for additional combinations of parameters are available in TABLE II of the Appendix.

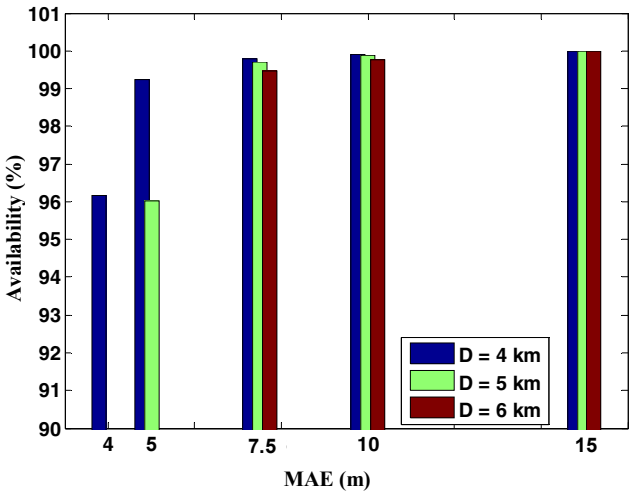


Figure 12. Additional airborne gemetry screening results using screening HAL: inflated $\sigma_{vig}$ and no inflation of $\sigma_{pr\_air}$.

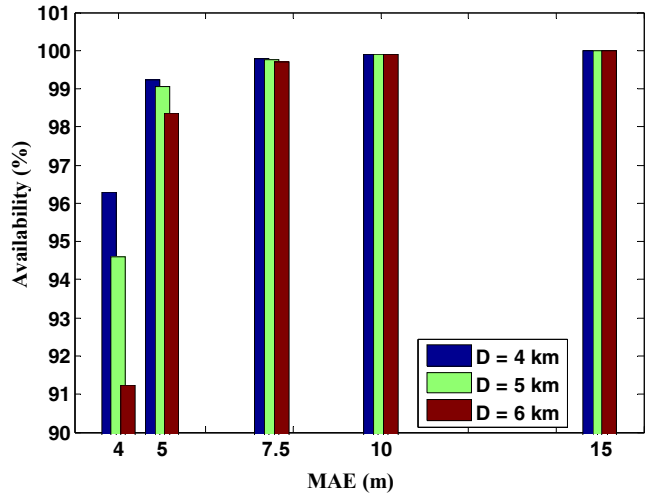


Figure 13. Additional airborne gemetry screening results using max. $|S_{horizontal}|$: inflated $\sigma_{vig}$ and no inflation of $\sigma_{pr\_air}$.

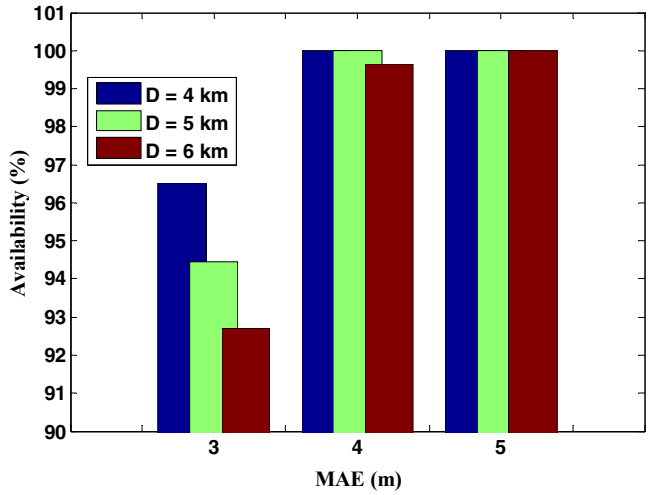


Figure 14. Additional airborne gemetry screening results for all-in-view geometries only using max. $|S_{horizontal}|$: inflated $\sigma_{vig}$ and no inflation of $\sigma_{pr\_air}$.

## VI. Conclusions and Future Work

Four conclusions have been drawn from the airport surface movement integrity requirement analyses conducted in this paper:

- If airport surface movement is defined as a separate operation from DCPS, it can be supported by the existing LGF geometry screening and by inflating $\sigma_{pr\_air}$ by a factor of 2 or more with the current integrity requirements for worst-case ionospheric anomalies.
- MAE with LGF geometry screening and $\sigma_{pr\_air}$ inflated by a factor of 2 can be reduced to 5 meters with 94.44% availability for all-in-view geometries and 7.5 meters with 97.96% availability for all *N*–1 gemetries for an LGF-to-user separation of 6 kilometers. Note that these results apply specifically to the Memphis LAAS installation, but similar availability should be obtainable elsewhere (simulations for other locations have not been performed yet).
- With the existing LGF geometry screening and current airborne $\sigma_{pr\_air}$, current airport surface movement integrity requirements cannot be met under anomalous ionosphere. Therefore, additional airborne geometry screening, implemented by limiting the "screening HAL" or the maximum $|S_{horizontal}|$ coefficient, is needed to fulfill the integrity requirements.
- MAE with LGF geometry screening and the current $\sigma_{pr\_air}$ can be reduced to 5 meters using a maximum $|S_{horizontal}|$ of 1.47 with 98.37% availability and 7.5 meters using a screening HAL of 5.69 with 99.47% availability. These results apply to all *N*–1 satellite geometries and a 6-kilometer separation.

Note that these conclusions are derived under the assumption of no nominal error contribution to HPE other than worst-case ionospheric errors. This assumption mirrors the model used for CAT I and is reasonable as long as anomalous ionosphere continues to be the dominant threat. However, in the surface-movement environment, worst-case airborne multipath might be a significant fraction of the worst-case ionospheric error. Limited data for airport surface movement exists at present, so examining multipath models for ground and obstruction-influenced specular and diffuse multipath is the first step in exploring this further. More data is expected to become available within the next year or two.

Taken together, these conclusions suggest that the approach described in this paper can support airport surface movement with useful MAEs of less than 10 meters and worthwhile availabilities of 95% or more. What makes this possible is removing airport surface movement from the domain of DCPS and defining it as an independent operation analogous to CAT I precision approach. While the separation of DCPS and surface movement is the most direct route to this objective, it may not be required if DCPS is enabled in a manner that does not limit availability based upon the worst-case ionospheric anomaly. One possibility, as proposed in [3], is to use information external to LAAS to separate periods in which worst-case errors are possible from the vast majority of times when the ionosphere is known to behave nominally.

## REFERENCES


[1] Y.S. Park, S. Pullen, and P. Enge, "Mitigation of Anomalous Ionosphere Threat to Enhance Utility of LAAS Differentially Corrected Positioning Service (DCPS)," *Proceedings of IEEE/ION PLANS 2008*, Monterey, CA, May 6-8, 2008.

[2] Y.S. Park, S. Pullen, and P. Enge, "Enabling the LAAS Differentially Corrected Positioning Service (DCPS): Design and Requirements Alternatives," *Proceedings of ION GNSS 2009*, Savannah, GA, September 22-25, 2009.

[3] T. Murphy, M. Harris, and Y.S. Park, S. Pullen, "GBAS Differentially Corrected Positioning Service Ionospheric Anomaly Errors Evaluated in an Operational Context," *Proceedings of ION ITM 2010*, San Diego, CA, January 25-27, 2010

[4] *Specification: Category I Local Area Augmentation System Ground Facility*. Washington, D.C., Federal Aviation Administration, FAA-E-2937A, April 17, 2002.

[5] *Minimum Aviation System Performance Standards for the Local Area Augmentation System (LAAS)*, Washington, D.C., RTCA SC-159, WG-4, DO-245A, December 9, 2004.

[6] *Minimum Operational Performance Standards for GPS Local Area Augmentation System Airborne Equipment*. Washington, D.C., RTCA SC-159, WG-4, DO-253C, December 16, 2008.

[7] J. Lee, M. Luo, S. Pullen, Y.S. Park, M. Brenner, and P. Enge, "Position-Domain Geometry Screening to Maximize LAAS Availability in the Presence of Ionosphere Anomalies," *Proceedings of ION GNSS 2006*, Fort Worth, TX, September 26-29 , 2006, pp. 393-408.

[8] ICAO Annex 10, "International Standards and Recommended Practices, - Aeronautical Telecommunications – Volume I (Radio Navigation Aids)", Amendment 77.

[9] S. Pullen, Y.S. Park, and P. Enge, "Impact and Mitigation of Ionospheric Anomalies on Ground Based Augmentation of GNSS," *Radio Science*, Vol. 44, August 2009.

[10] S. Ramakrishnan, J. Lee, S. Pullen, and P. Enge, "Targeted Ephemeris Decorrelation Parameter Inflation for Improved LAAS Availability during Severe Ionosphere Anomalies," *Proceedings of the 2008 National Technical Meeting*, San Diego, CA, January 24-26, 2008.

[11] D.V. Simili, B. Pervan, "Code-Carrier Divergence Monitoring for the GPS Local Area Augmentation System, *Proceedings of IEEE/ION PLANS 2006*, San Diego, CA, April 25-27, 2006.

[12] C. Shively, "Safety Concepts for Mitigation of Ionospheric Anomaly Errors in GBAS", *Proceedings of ION NTM 2008*, San Diego, CA, January 28-30, 2008.

## APPENDIX

TABLE I. AVAILABILITY WITH ADDITIONAL GEOMETRY SCREENING: NO SIGMA INFLATION

| MAE (m) | LGF-to-User Separation (km) | Rule 1: Screening HAL | | | Rule 2: Maximum $\lvert S_{horizontal} \rvert$ | | |
|---|---|---|---|---|---|---|---|
| | | *Screening HAL (m)* | *Availability for all-in-view geometries (%)* | *Availability for N-1 geometries (%)* | *Max. $\lvert S_{horizontal} \rvert$* | *Availability for all-in-view geometries (%)* | *Availability for N-1 geometries (%)* |
| 3 | 1 | N/A[a] | 100 | 95.08 | N/A | 100 | 95.08 |
| | 2 | N/A | 100 | 94.75 | N/A | 100 | 94.75 |
| | 3 | 2.85 | 100 | 91.09 | 1.43 | 100 | 94.38 |
| | 4 | 2.48 | 96.18 | 79.57 | 1.18 | 99.65 | 91.45 |
| | 5 | 2.23 | 91.32 | 64.31 | 1.01 | 97.22 | 85.92 |
| | 6 | 2.02 | 76.39 | 38.26 | 0.89 | 94.79 | 76.68 |
| 4 | 1 | N/A | 100 | 99.10 | N/A | 100 | 99.10 |
| | 2 | N/A | 100 | 99.06 | N/A | 100 | 99.06 |
| | 3 | 3.88 | 100 | 98.82 | 1.89 | 100 | 98.94 |
| | 4 | 3.25 | 100 | 96.30 | 1.57 | 100 | 98.66 |
| | 5 | 2.78 | 100 | 87.63 | 1.35 | 100 | 97.48 |
| | 6 | 2.59 | 96.53 | 80.50 | 1.18 | 99.65 | 94.02 |
| 5 | 1 | N/A | 100 | 99.67 | N/A | 100 | 99.67 |
| | 2 | N/A | 100 | 99.64 | N/A | 100 | 99.63 |
| | 3 | 4.98 | 100 | 99.64 | 2.37 | 100 | 99.63 |
| | 4 | 4.10 | 100 | 99.06 | 1.96 | 100 | 99.59 |
| | 5 | 3.42 | 100 | 97.03 | 1.68 | 100 | 99.43 |
| | 6 | 3.20 | 100 | 94.99 | 1.47 | 100 | 98.94 |
| 7.5 | 1 | N/A | 100 | 99.88 | N/A | 100 | 99.88 |
| | 2 | N/A | 100 | 99.88 | N/A | 100 | 99.88 |
| | 3 | N/A | 100 | 99.88 | N/A | 100 | 99.88 |
| | 4 | 6.10 | 100 | 99.84 | 2.95 | 100 | 99.88 |
| | 5 | 5.53 | 100 | 99.72 | 2.53 | 100 | 99.88 |
| | 6 | 4.83 | 100 | 99.59 | 2.21 | 100 | 99.80 |
| 10 | 1 | N/A | 100 | 99.96 | N/A | 100 | 99.96 |
| | 2 | N/A | 100 | 99.96 | N/A | 100 | 99.96 |
| | 3 | N/A | 100 | 99.96 | N/A | 100 | 99.96 |
| | 4 | 8.66 | 100 | 99.92 | 3.92 | 100 | 99.96 |
| | 5 | 7.49 | 100 | 99.88 | 3.36 | 100 | 99.92 |
| | 6 | 6.48 | 100 | 99.84 | 2.95 | 100 | 99.92 |
| 15 | 1 | N/A | 100 | 100 | N/A | 100 | 100 |
| | 2 | N/A | 100 | 100 | N/A | 100 | 100 |
| | 3 | N/A | 100 | 100 | N/A | 100 | 100 |
| | 4 | 13.46 | 100 | 100 | 5.89 | 100 | 100 |
| | 5 | 11.23 | 100 | 100 | 5.06 | 100 | 100 |
| | 6 | 10.26 | 100 | 99.96 | 4.43 | 100 | 100 |
| 20 | 1 | N/A | 100 | 100 | N/A | 100 | 100 |
| | 2 | N/A | 100 | 100 | N/A | 100 | 100 |
| | 3 | N/A | 100 | 100 | N/A | 100 | 100 |
| | 4 | 17.55 | 100 | 100 | 7.89 | 100 | 100 |
| | 5 | 15.77 | 100 | 100 | 6.77 | 100 | 100 |
| | 6 | 13.83 | 100 | 100 | 5.89 | 100 | 100 |

a. "N/A" means no additional geometry restriction.

TABLE II. AVAILABILITY WITH ADDITIONAL GEOMETRY SCREENING: INFLATED $\sigma_{vig}$ AND NO INFLATION OF AIRBORNE $\sigma_{pr\_air}$

| MAE (m) | LGF-to-User Separation (km) | Rule 1: Screening HAL | | | Rule 2: Maximum $\lvert S_{horizontal} \rvert$ | | |
|---|---|---|---|---|---|---|---|
| | | *Screening HAL (m)* | *Availability for all-in-view geometries (%)* | *Availability for N-1 geometries (%)* | *Max. $\lvert S_{horizontal} \rvert$* | *Availability for all-in-view geometries (%)* | *Availability for N-1 geometries (%)* |
| 3 | 1 | N/A[a] | 98.26 | 85.51 | N/A | 98.26 | 85.51 |
| | 2 | N/A | 97.92 | 84.17 | N/A | 97.92 | 84.17 |
| | 3 | N/A | 96.53 | 81.93 | N/A | 96.53 | 81.93 |
| | 4 | 2.95 | 96.53 | 78.47 | 1.20 | 96.53 | 79.81 |
| | 5 | 2.60 | 83.33 | 56.90 | 1.01 | 94.44 | 75.91 |
| | 6 | 2.34 | 55.56 | 29.87 | 0.89 | 92.71 | 68.42 |
| 4 | 1 | N/A | 100 | 97.68 | N/A | 100 | 97.68 |
| | 2 | N/A | 100 | 97.44 | N/A | 100 | 97.44 |
| | 3 | N/A | 100 | 96.95 | N/A | 100 | 96.95 |
| | 4 | 3.99 | 100 | 96.17 | 1.60 | 100 | 96.30 |
| | 5 | 3.38 | 97.57 | 86.32 | 1.35 | 100 | 94.59 |
| | 6 | 3.01 | 94.10 | 73.18 | 1.18 | 99.65 | 91.25 |
| 5 | 1 | N/A | 100 | 99.55 | N/A | 100 | 99.55 |
| | 2 | N/A | 100 | 99.51 | N/A | 100 | 99.51 |
| | 3 | N/A | 100 | 99.43 | N/A | 100 | 99.43 |
| | 4 | N/A | 100 | 99.23 | 2.14 | 100 | 99.23 |
| | 5 | 4.11 | 100 | 96.01 | 1.69 | 100 | 99.06 |
| | 6 | 3.72 | 99.31 | 89.62 | 1.47 | 100 | 98.37 |
| 7.5 | 1 | N/A | 100 | 99.84 | N/A | 100 | 99.84 |
| | 2 | N/A | 100 | 99.84 | N/A | 100 | 99.84 |
| | 3 | N/A | 100 | 99.84 | N/A | 100 | 99.84 |
| | 4 | N/A | 100 | 99.80 | N/A | 100 | 99.80 |
| | 5 | 6.73 | 100 | 99.72 | 2.53 | 100 | 99.76 |
| | 6 | 5.69 | 100 | 99.47 | 2.21 | 100 | 99.72 |
| 10 | 1 | N/A | 100 | 99.96 | N/A | 100 | 99.96 |
| | 2 | N/A | 100 | 99.96 | N/A | 100 | 99.96 |
| | 3 | N/A | 100 | 99.96 | N/A | 100 | 99.96 |
| | 4 | N/A | 100 | 99.92 | N/A | 100 | 99.92 |
| | 5 | 8.96 | 100 | 99.88 | 3.38 | 100 | 99.92 |
| | 6 | 7.71 | 100 | 99.76 | 2.95 | 100 | 99.92 |
| 15 | 1 | N/A | 100 | 100 | N/A | 100 | 100 |
| | 2 | N/A | 100 | 100 | N/A | 100 | 100 |
| | 3 | N/A | 100 | 100 | N/A | 100 | 100 |
| | 4 | N/A | 100 | 100 | N/A | 100 | 100 |
| | 5 | 13.64 | 100 | 100 | 5.14 | 100 | 100 |
| | 6 | 12.14 | 100 | 100 | 4.43 | 100 | 100 |
| 20 | 1 | N/A | 100 | 100 | N/A | 100 | 100 |
| | 2 | N/A | 100 | 100 | N/A | 100 | 100 |
| | 3 | N/A | 100 | 100 | N/A | 100 | 100 |
| | 4 | N/A | 100 | 100 | N/A | 100 | 100 |
| | 5 | 18.78 | 100 | 100 | 6.78 | 100 | 100 |
| | 6 | 16.79 | 100 | 100 | 5.89 | 100 | 100 |

a. "N/A" means no additional geometry restriction.

TABLE III. SENSITIVITY OF AVAILABILITY TO AIRBORNE $\sigma_{pr\_air}$ INFLATION: INFLATED $\sigma_{vig}$

| MAE (m) | LGF-to-User Separation (km) | Availability (%) | | | | | | | |
|---|---|---|---|---|---|---|---|---|---|
| | | *1.5 $\sigma_{pr\_air}$* | | *2 $\sigma_{pr\_air}$* | | *3 $\sigma_{pr\_air}$* | | *4 $\sigma_{pr\_air}$* | |
| | | *All-in-view geometries* | *N-1 geometries* | *All-in-view geometries* | *N-1 geometries* | *All-in-view geometries* | *N-1 geometries* | *All-in-view geometries* | *N-1 geometries* |
| 4 | 1 | 97.22 | 82.34 | 84.33 | [a] | | | | |
| | 2 | 97.22 | 81.93 | 80.56 | | | | | |
| | 3 | 96.53 | 80.55 | 77.08 | | | | | |
| | 4 | 96.18 | 79.20 | 73.26 | | | | | |
| | 5 | 95.83 | 77.57 | 69.10 | | | | | |
| | 6 | 94.44 | 75.86 | 64.58 | | | | | |
| 5 | 1 | 100 | 95.73 | 96.18 | 79.65 | | | | |
| | 2 | 100 | 95.60 | 95.49 | 79.08 | | | | |
| | 3 | 100 | 95.08 | 95.14 | 78.35 | | | | |
| | 4 | 100 | 94.30 | 95.14 | 77.33 | | | | |
| | 5 | 100 | 93.28 | 95.14 | 76.56 | | | | |
| | 6 | 100 | 91.82 | 94.44 | 75.42 | | | | |
| 7.5 | 1 | 100 | 99.59 | 100 | 98.37 | 96.88 | 81.64 | 72.57 | |
| | 2 | 100 | 99.59 | 100 | 98.33 | 96.88 | 81.60 | 72.22 | |
| | 3 | 100 | 99.59 | 100 | 98.33 | 96.88 | 81.36 | 71.88 | |
| | 4 | 100 | 99.59 | 100 | 98.13 | 96.53 | 81.03 | 70.83 | |
| | 5 | 100 | 99.55 | 100 | 98.09 | 96.53 | 80.71 | 69.79 | |
| | 6 | 100 | 99.55 | 100 | 97.76 | 96.18 | 80.10 | 67.71 | |
| 10 | 1 | 100 | 99.84 | 100 | 99.59 | 100 | 96.99 | 97.57 | 82.38 |
| | 2 | 100 | 99.84 | 100 | 99.59 | 100 | 96.91 | 97.22 | 82.25 |
| | 3 | 100 | 99.84 | 100 | 99.59 | 100 | 96.78 | 97.22 | 82.09 |
| | 4 | 100 | 99.80 | 100 | 99.59 | 100 | 96.74 | 97.22 | 81.85 |
| | 5 | 100 | 99.80 | 100 | 99.59 | 100 | 96.66 | 97.22 | 81.77 |
| | 6 | 100 | 99.76 | 100 | 99.59 | 100 | 96.58 | 96.88 | 81.60 |
| 15 | 1 | 100 | 99.96 | 100 | 99.88 | 100 | 99.63 | 100 | 98.70 |
| | 2 | 100 | 99.96 | 100 | 99.88 | 100 | 99.63 | 100 | 98.70 |
| | 3 | 100 | 99.96 | 100 | 99.88 | 100 | 99.63 | 100 | 98.70 |
| | 4 | 100 | 99.96 | 100 | 99.88 | 100 | 99.63 | 100 | 98.62 |
| | 5 | 100 | 99.96 | 100 | 99.88 | 100 | 99.59 | 100 | 98.58 |
| | 6 | 100 | 99.96 | 100 | 99.88 | 100 | 99.59 | 100 | 98.58 |
| 20 | 1 ~ 6 | 100 | 100 | 100 | 99.96 | 100 | 99.84 | 100 | 99.64 |
| 25 | 1 ~ 6 | 100 | 100 | 100 | 100 | 100 | 99.88 | 100 | 99.84 |
| 30 | 1 ~ 6 | 100 | 100 | 100 | 100 | 100 | 99.96 | 100 | 99.88 |

a. Availability for the empty cell is less than 50 %.